Electronic Supplementary Material (ESI) for Journal of Materials Chemistry A.

Supplementary Materials for

Massively Enhanced Ionic Transport in Irradiated Crystalline Pyrochlore

C.R. Kreller[a]*, J.A. Valdez[b], T.G. Holesinger[c], J. Morgan[d], Y.Q. Wang[b], M. Tang[b], F.G. Garzon[e], R. Mukundan[a], E.L. Brosha[a], B.Uberuaga[b]

[a]*MPA-11: Materials Synthesis and Integrated Devices, Los Alamos National Laboratory, Los Alamos, NM 87545.*
[b]*MST-8: Materials Science in Radiation and Dynamics Extremes, Los Alamos National Laboratory, Los Alamos, NM 87545.*
[c]*MST-16: Nuclear Materials Science, Los Alamos National Laboratory, Los Alamos, NM 87545.*
[d]*Department of Materials Science & Engineering, University of Sheffield, Sheffield S10 2TN, UK*
[e]*Advanced Materials Laboratory, University of New Mexico, Albuquerque, NM 87106*
*correspondence to: ckreller@lanl.gov

This PDF file includes:

Materials and Methods

Target synthesis and characterization

Details on target preparation and film growth are given elsewhere and briefly summarized here[1]. $Gd_2Ti_2O_7$ was synthesized via solid-state methods from high purity Gd_2O_3 and TiO_2. Powders were mixed in an inert atmosphere glove box, milled for 6 hours in a Retsch rotary mill, dried on a shlink line, and then calcined as a loose powder for 10 hours under 25%O2/ Ar gas flow at 700°C. A 2-inch diameter target was prepared by uniaxial pressing at 15lbs followed by sintering at 1575˚C for 100 hours in an oxygen atmosphere furnace on a bed of loose powder in a high purity alumina boat.

RF magnetron sputtering

Thin films were prepared using RF magnetron sputtering on 111 oriented single crystal YSZ substrates (8 mol% Y2O3 stabilized ZrO2, one-side polished, MTI corporation). Substrates were affixed to the faceplate of a Ni heater box using Ag paste (Aremco). A photo lamp heater bulb (Wiko) was used to maintain the faceplate at 800˚C during deposition. The heater box was mounted off-axis with the faceplate distanced 3.5 inches from the target. Films were grown in 50%O_2/balance Ar atmosphere with total pressure maintained at 25mTorr and at a power setting of 100W. These sputtering conditions yielded a deposition rate of roughly 17Å/min.

Thin films of 400-500nm thickness were utilized in order to measure the damaged material in isolation. The irradiation conditions were chosen such that the implanted He resided primarily in the YSZ substrate (Fig. S1). YSZ was selected as the substrate because it provides excellent lattice matching for growing the epitaxial pyrochlore structure, with lattice misfit of only $\delta=(a_{GTO}/2-a_{YSZ})/a_{YSZ}*100\%=-.63\%$ (a_{GTO}=10.185A and a_{YSZ}=5.125A). Additionally, the conductivity of the YSZ and the geometric aspect ratio of the experiment provided clear separation of the AC impedance response of the GTO thin film in through-plane measurements. YSZ is also a very radiation tolerant material and its structure and transport properties were unaffected by the He irradiations used in this study, as confirmed by conductivity measurements of the bare YSZ substrate exposed to a fluence of 8 $x10^{16}$ He/cm^2.

Irradiation

Light ion irradiation conditions, predominantly creating isolated Frenkel pairs, were used in order to induce disorder on the cation and anion sublattices, rather than completely amorphize the material. Bombardment of a material with such low energy He ions with energy in the nuclear stopping range yields a damage profile with increasing damage with increasing depth up to a maximum displacements per atom (DPA) at a depth of approximately 600nm (Fig. S1)[2].

The irradiations were done with 200 keV He^+ ions using a Danfysik Research Ion implanted at the Ion Beam Materials Laboratory at Los Alamos National Laboratory. The irradiation flux was -1.5 x 10^{13} ions•cm^{-2}•s^{-1}. The irradiations were done at room temperature. The target was actively cooled with high-pressure air during the implantation. The temperature was monitored on the target holder using thermal couples,

which indicated that the temperature rise during irradiation was never greater than 35˚C. The vacuum in the chamber was kept below $5x10^{-7}$ torr to minimize any deposition of hydrocarbons on the surface.

The damage and implantation profiles were estimated using the Stopping and Range of Ions in Matter (SRIM) Monte Carlo Code.[3] The displacement threshold energy for all species was assumed to be 40 eV. The density of the target sample was taken as 6.66 g/cm^3. The predicted damage profile for 200keV He ions in GTO is shown in Fig. S1. The peak He implantation depth was 200-300nm deeper than the GTO/YSZ interface depth, indicating that the vast majority of He is implanted into the YSZ substrate.

Materials Characterization

Phase purity of the sintered target was confirmed by powder X-ray diffraction (XRD). Films were characterized by grazing incidence X-ray diffraction (GIXRD) and transmission electron microscopy (TEM). GIXRD measurements were performed using a Bruker AXS D8 Advance X-ray diffractometer, with a Cu-K_α radiation (λ=1.5406Å) X-ray source operating in θ-2θ geometry, and at the fixed angle of incidence (γ) of 0.75° relative to the specimen surface. This angle of incidence corresponds to probing the top 135nm of the material, approximately, as shown in Fig. S1. The X-ray diffractometer exit source was equipped with a Göebel mirror diffraction optic used to achieve a parallel beam condition that is highly sensitive to near surface features in thin films. The θ-2θ scans were performed using a step size of 0.02° and a dwell time of 4 s per step. Diffracted intensities from the specimens were collected using a solid-state detector to suppress fluorescence from the rare-earth gadolinium constituent.

A typical diffraction pattern of an as-deposited film is shown in **Fig S2a**. Due to the textured nature of the films grown on 111 YSZ, the diffraction patterns exhibited poor signal to noise with significant peak broadening. The structure of the thin films is nearly single-crystalline. In order to characterize the disorder, we require the intensity of multiple Bragg peaks, corresponding to different grain orientations. As the diffractometer did not have a sample tilting stage, it essentially does not average over a wide range of grain orientations in such a sample and thus the diffraction pattern is too strongly representative of a single grain orientation, making comparison of peak intensities impossible. Thus, XRD characterization was carried out on polycrystalline bulk samples irradiated under the same conditions as the thin films to overcome this limitation of our system.

Diffraction patterns of the bulk material irradiated at select fluences are shown in **Fig S2b**. As the pyrochlore is a superstructure of the defect fluorite phase, the peak intensities of the pyrochlore diffraction patterns decrease as the material becomes less ordered while those of the parent fluorite structure remain constant. Therefore, as shown by previous authors, the ratio of intensities of the primary pyrochlore diffraction peak to that of the primary fluorite diffraction peak can be used as a proxy for estimating average cation disorder[4]. The ratio of the intensities of the pyrochlore (331) and the defect fluorite (400) peaks were used to calculate the percent cation disorder. This calculation involved simulating the diffraction pattern of hypothetical structures with varying amounts of disorder, similar to what was done by Moon and Tuller[4]. We created structures in which

both the cation and anion sublattices were independently randomized to various degrees of disorder. The diffraction pattern of the resulting structure was simulated using CrystalMaker and CrystalDiffract[5]. Peak ratios were extracted from these simulations and correlated with the experimental peak ratios. The disorder of the simulated structure was then assigned to the experimental material. We note that recent experiments have found that irradiated pyrochlores exhibit significant short range order, which complicates the creation of representative disordered structures[6] However, the long range order, as probed by XRD, has been shown by the same authors to be similar to disordered fluorite. This provides confidence that, for an average change in disorder, this procedure is accurate. Between a fluence of $5x10^{16}$ and $8x10^{16}$ He/cm^2, peak broadening and diffuse scattering around the [311] and [222] Bragg peaks indicated the onset of amorphization. Further, the pyrochlore [331] peak could not be sufficiently distinguished from the background of the neighboring [400] fluorite peak. This result suggests that GTO can tolerate approximately 50% cation disorder before the high anti-site defect formation energy results in amorphization of the material.

The structure of the films was examined in a FEI Titan 300kV image corrected (scanning) transmission electron microscope (S/TEM). Specimens for S/TEM analysis were prepared via a focused ion beam (FIB) process. The specimen was cut from the film, plucked and attached to a copper FIB grid, and then thinned to electron transparency.

Conductivity measurements

A schematic illustrating the experimental set-up for AC impedance measurements is shown in **Fig. S3**. In order to provide electrical contact for performing AC impedance measurements, a counter electrode was prepared by affixing Pt-foil to the backside of the YSZ substrate using Pt ink (ESL Electroscience) cured at 900˚C. Patterned Pt-electrodes of 0.1-1mm in diameter were sputtered onto the GTO film surface using a shadow mask (Photo Etch). The thin film assembly was loaded into a high temperature crucible (Linkham) mounted on a microprobe station (Cascade Microtech). Gold-coated tungsten probe tips were contacted to the Pt-foil counter electrode and a Pt-working electrode on the surface of the GTO film. AC impedance measurements were performed using a PARSTAT 2273 potentiostat/FRA in the frequency range of 10^6-0.1 Hz as a function of temperature (500-900˚C) in ambient gas environment.

The spectra obtained from AC impedance measurements yielded three distinct features when plotted in Nyquist form, as shown in **Fig. S4**. The low frequency arc is due to interfacial processes (Pt||GTO, GTO||YSZ, YSZ||Pt) and was not included in the analysis. The intermediate frequency arc was of primary interest and was attributed to the GTO thin film. The high frequency intercept yields the ohmic resistance of the YSZ substrate, as electronic resistances were minimal. Fits to the high and intermediate frequency features were performed using ZView with an equivalent circuit of the form shown in the inset of **Fig. S4**. Fitting using a constant phase element (CPE) rather than a pure capacitor yielded similar values for the resistance of the intermediate frequency arc. Values from both equivalent circuit fittings are used in the calculations of the average

conductivities. The conductivity was calculated from the fitted resistance values using the relationship:

$$\sigma_{GTO} = \frac{1}{R_{GTO}} \frac{L}{A} \qquad (1)$$

where σ is conductivity in S•cm^{-1}, R is the resistance in Ω, A is the cross sectional area of the microelectrode in cm^2 and L is thickness of the GTO thin film in cm.

Details on verifying the correctness of the equivalent circuit assignments are provided in a prior publication[1]. In short, the high frequency intercept yielded conductivity values that matched that of the YSZ substrate measured independently. Fitting of the intermediate frequency arc yielded capacitance values that scaled as expected with film thickness and conductivity values from films of two different thicknesses that were similar to that measured on a bulk GTO pellet.

Impedance measurements were performed on GTO thin films exposed to irradiation fluences of 1x10^{13}, 1x10^{14}, 1x10^{15}, 1x10^{16}, 8x10^{16} and 9x10^{16} He•cm^{-2}. Measurements were made between 500-900˚C in 50˚C increments on multiple microelectrodes on a given film. At least two temperature cycles were recorded for every sample and no hysteresis was observed, indicating that the irradiation induced disorder is not annealed out under the time and temperature of the experimental data collection. The persistence of the disorder upon thermal cycling up to 900˚C is consistent with the Raman and XAS study performed by Sanjuan et al.[7] that showed that while some ordering occurred in mechanically milled amorphous GTO between 700-800˚C, a completely ordered structure was not achieved after heating to 900˚C. The data points in **Fig. 3** are the average of the data collected on multiple microelectrodes of varying diameter over multiple temperature cycles with corresponding error bars representing the standard deviations. Pristine films of two different thicknesses were measured to ensure that in films of 400-500nm thickness, any interfacial strain effects have relaxed and are not influencing the measured conductivity[1].

The data in **Fig. 3** were fit to the Arrhenius equation:

$$\sigma = \frac{\sigma_o}{T} Exp\left(\frac{-E_A}{kT}\right)$$

Where, σ (Scm^{-1}) is the average conductivity, T (K) is the temperature, σ_o (S•cm^{-1}) is the pre-exponential constant, E_A is the activation energy of the bulk conduction process, and k is the Boltzmann constant (8.617x10^{-5} eV•K^{-1}).

The impedance of a pristine sample and a sample irradiated at 1 x 10^{16} He•cm^{-2} was also measured as a function of oxygen partial pressure in a sealed tube furnace by spot welding Pt wires onto a 1mm electrode on the GTO surface and the Pt-foil on the

underside of the YSZ substrate. Gas mixtures were supplied to the furnace at a total flow rate of 100ccm using MKS mass flow controllers. UHP oxygen and UHP nitrogen were used for pO_2=1 and 0.21. A specialty mixture of 2% Oxygen in argon was mixed with UHP nitrogen for pO_2= 10^{-2} and 10^{-3}. UHP argon was used for pO_2=10^{-6}. The pristine sample was measured at 610, 710 and 810 ˚C (as measured with a thermocouple, which was offset from the furnace temperature by 10˚C). The sample irradiated at 1 x 10^{16} He•cm^{-2} was measured at 610 and 710˚C. This sample was not measured at 810˚C because the frequency range of the impedance analyzer was insufficient to capture enough of the intermediate frequency arc attributed to GTO to yield reasonable equivalent circuit fitting at this temperature and with the 1mm diameter electrode. The results of the pO_2 dependent measurements are shown in Fig. S5.

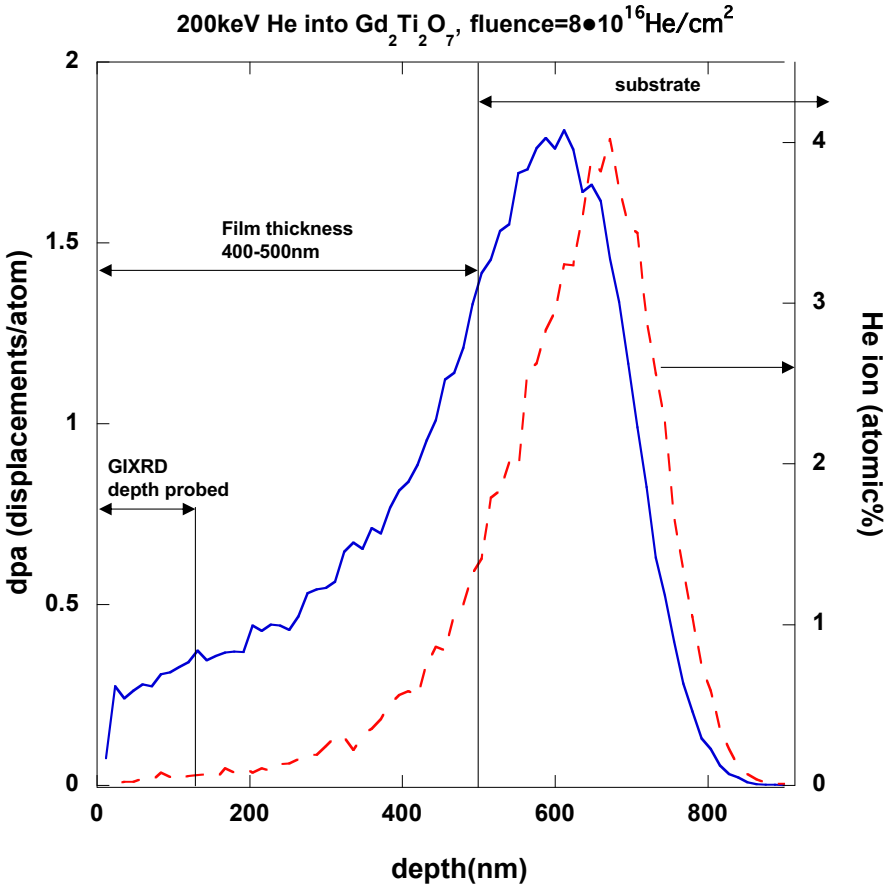

Fig. S1

SRIM calculation of DPA as a function of depth for 200keV He ions in GTO shown on primary y-axis (solid blue line). Corresponding atomic % of implanted He shown on secondary y-axis (dashed red line).

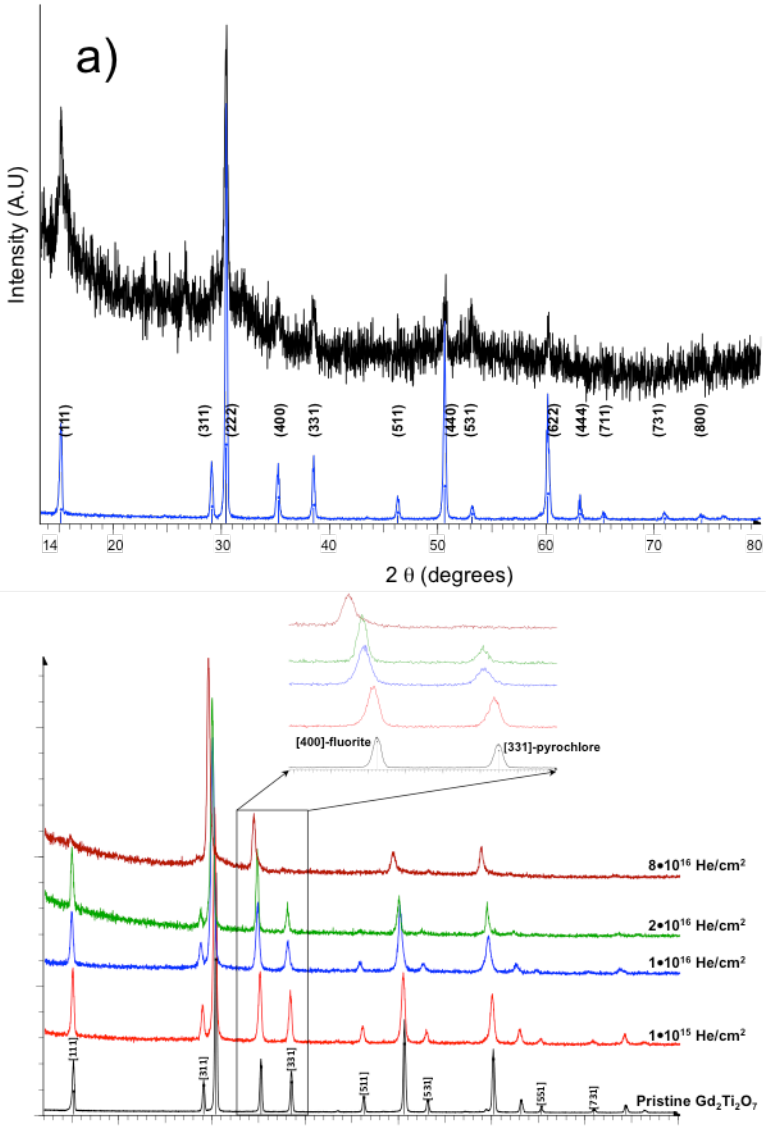

Fig. S2.

(a) Diffraction pattern of pristine GTO thin film and (b) Diffraction patterns of pristine and irradiated bulk GTO obtained from grazing incidence x-ray diffraction at an angle of 0.75˚. Labels correspond to pyrochlore supercell reflections.

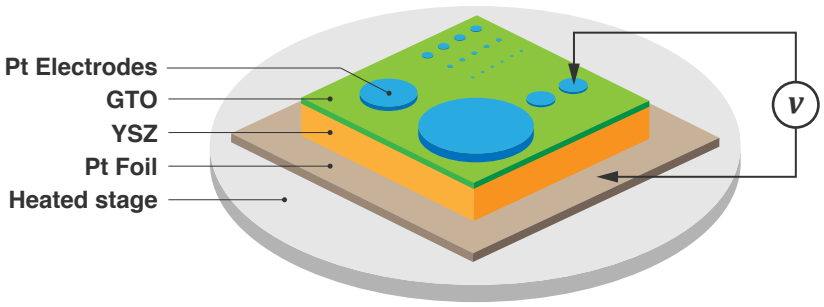

Fig. S3

Schematic illustrating AC impedance measurement.

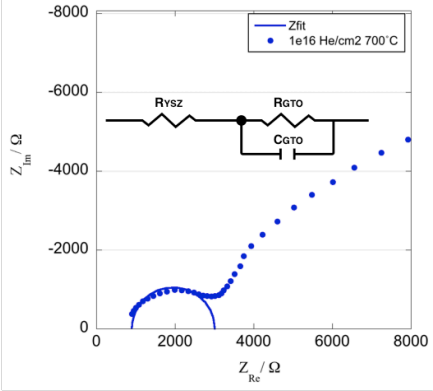

Fig. S4

Impedance spectra of thin film irradiated at 1 x 10^{16} He•cm^{-2} at 700˚C. Data obtained using 2-probe through plane measurement between 1mm diameter working electrode and counter electrode. Inset shows equivalent circuit used to fit high and intermediate frequency response (solid line) in ZView. Low frequency response attributed to interfacial reactions and not included in this analysis.

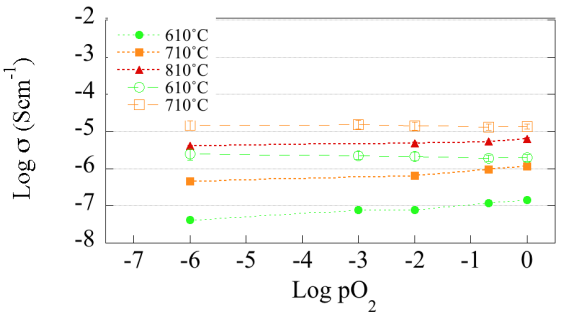

Fig. S5

Conductivity as a function of pO_2 and temperature for pristine film (filled data points) and film irradiated at 1 x 10^{16} He•cm^{-2} (open data points). Lines are intended as guides for the eye and were not obtained by fitting to a chemical defect model.

References:

1. C. R. Kreller, J. A. Valdez, T. G. Holesinger, R. Mukundan, E. L. Brosha, T. Williamson, Y. Q. Wang and B. P. Uberuaga, *Solid State Ionics*, 2018, **314**, 36-40.
2. J. F. Ziegler, M. D. Ziegler and J. P. Biersack, *Nuclear Instruments and Methods in Physics Research Section B: Beam Interactions with Materials and Atoms*, 2010, **268**, 1818-1823.
3. J. F. Ziegler, J. P. Biersack and U. Littmark, *The Stopping and Range of Ions in Solids*, Pergamon, 1985.
4. P. K. Moon and H. L. Tuller, *Materials Research Society Symposium Proceedings*, 1989, **135**, 149-163.

5. D. Simeone, G. J. Thorogood, D. Huo, L. Luneville, G. Baldinozzi, V. Petricek, F. Porcher, J. Ribis, L. Mazerolles, L. Largeau, J. F. Berar and S. Surble, *Sci Rep*, 2017, **7**, 7.
6. J. Shamblin, M. Feygenson, J. Neuefeind, C. L. Tracy, F. X. Zhang, S. Finkeldei, D. Bosbach, H. D. Zhou, R. C. Ewing and M. Lang, *Nat Mater*, 2016, **15**, 507-+.
7. M. L. Sanjuán, C. Guglieri, S. Díaz-Moreno, G. Aquilanti, A. F. Fuentes, L. Olivi and J. Chaboy, *Physical Review B*, 2011, **84**, 104207.